

A STUDY OF HIGH MASS e^+e^- PAIRS PRODUCED IN p-p COLLISIONS

AT THE CERN ISR

[CERN¹-Columbia²-Oxford³-Rockefeller⁴ (CCOR) Collaboration]

A.L.S. Angelis³, B.J. Blumenfeld², L. Camilleri¹, T.J. Chapin⁴,
R.L. Cool⁴, C. del Papa¹, L. Di Lella¹, Z. Dimčovski⁴,
R.J. Hollebeek², D. Levinthal², L.M. Lederman², J.T. Linnemann⁴,
L. Lyons³, N. Phinney³, B.G. Pope^{1*}, S.H. Pordes¹, A.F. Rothenberg^{4**},
A.M. Segar³, J. Singh-Sidhu¹, A.M. Smith¹, M.J. Tannenbaum⁴,
R.A. Vidal^{2***}, J. Wallace-Hadrill³, T.O. White^{3†} and J.M. Yelton³

ABSTRACT

An apparatus consisting of a superconducting solenoidal magnet, cylindrical drift chambers, and two arrays of lead-glass Čerenkov counters has been used at the CERN ISR to study the production of e^+e^- pairs of invariant mass larger than $6 \text{ GeV}/c^2$.

Measurements of $(d^2\sigma/dm dy)_{y=0}$ for the e^+e^- continuum and of $B(d\sigma/dy)_{y=0}$ for the T resonances will be presented for $\sqrt{s} = 62.4 \text{ GeV}$. The mean p_T of the e^+e^- pairs and the multiplicity and momentum spectrum of associated particles will be discussed.

CERN LIBRARIES, GENEVA



CM-P00064009

Geneva - 20 September 1978

Submitted to the
19th International Conference on High-Energy Physics,
Tokyo, August 1978

-
- *) Present address: Physics Dept., Princeton University, New Jersey, USA.
 - **) Present address: CERN, Geneva, Switzerland.
 - ***) Present address: Stanford Linear Accelerator Center, Stanford, Calif., USA.
 - †) Present address: Cavendish Laboratory, University of Cambridge, UK.

1. INTRODUCTION

The behaviour of the cross-section for the production of high-mass lepton pairs in pp collisions as a function of \sqrt{s} is a topic of current interest. A measurement of the production cross-section of the recently discovered Υ resonances¹⁾ as a function of \sqrt{s} would shed light on the production mechanism involved. The large \sqrt{s} available at the CERN Intersecting Storage Rings (ISR) makes it a suitable place for addressing these questions.

This paper presents data collected at the ISR on the production of electron pairs

$$p + p \rightarrow e^+ + e^- + X$$

at a c.m. energy of 62.4 GeV. The mass region covered is $m > 6 \text{ GeV}/c^2$. Cross-sections in the form $(d^2\sigma/dm dy)_{y=0}$ and results on the mean transverse momentum $\langle p_T \rangle$ of the pairs and on the particles associated with the pairs are presented.

2. APPARATUS

The apparatus (Fig. 1) consists of a 1.5 tesla superconducting solenoid containing drift chambers, and of two lead-glass arrays located outside the magnet.

The solenoid coil is aluminium stabilized and has a thickness corresponding to one radiation length of aluminium. The inner dimensions of the solenoid are: radius = 70 cm, length = 170 cm. The field uniformity is $\pm 1.5\%$ over the volume of the drift chambers. The iron return yoke is built in such a way as to leave two windows obstructed only by the coil. Each window covers a laboratory angle of $45^\circ < \theta < 135^\circ$ and 90° in ϕ .

The drift chamber system²⁾ surrounds the vacuum pipe and consists of four modules DCM1-DCM4; each module contains two gaps. The sense wires run parallel to the magnetic field, and hence the drift times provide the ϕ coordinates of charged tracks. This is the coordinate that requires the highest accuracy because it is in the bending plane of the magnet. Delay lines are glued to the cathode planes facing each of the 580 sense wires. The times of arrival at the two ends

of the delay lines of the pulses induced on these delay lines give the z coordinate along the solenoid axis. The system thus provides pairs of ϕ , z coordinates, reducing off-line computer usage by eliminating the need for ϕ , z matching. Within a module, the sense wires of one gap are displaced with respect to the sense wires of the other gap by one half the sense-sense distance. This resolves most of the left/right sense wire ambiguities.

A lead-glass wall consisting of 168 blocks arranged in a 12×14 array is located behind each of the two windows in the solenoid. Each block has a cross-sectional area of 15×15 cm and is 40 cm thick (17 r.l.). The front face of each wall is located at 120 cm from the intersection region. To reduce the effect of the fringing field of the solenoid on the photomultipliers, a 6 mm thick iron plate is mounted on the front face of the arrays. Each block has been calibrated in an electron beam at the CERN Proton Synchrotron (PS). A small NaI crystal doped with ^{241}Am is glued to the front face of each block³⁾. The pulse height of the light emitted by these crystals is recorded after every ISR run, thus providing a constant monitoring of this calibration. Two further checks on the calibration of each block are made:

- i) the pulse-height spectrum resulting from the traversal of a block by hadrons is monitored;
- ii) the lead-glass wall is positioned at 350 cm, and the π^0 mass is reconstructed from events where the two γ 's are well separated.

It is estimated that the over-all absolute energy calibration is known to $\pm 5\%$.

Two scintillator hodoscopes A and B are used. Hodoscope A, a "barrel" of 32 counters, is mounted between DCM1 and DCM2. It is used to provide, event by event, a zero time relative to which the drift chamber times are measured. Hodoscope B is mounted against the outer face of the coil and consists of one 12-counter array in front of each of the two thin windows of the solenoid. In this analysis it was used to measure the number of particles emerging from the coil along the electron candidate track. All A and B scintillators are equipped with photomultipliers at both ends, and the pulse heights from all phototubes are recorded.

The stainless-steel vacuum pipe has an average thickness of 0.36 mm (0.02 radiation lengths).

3. TRIGGER

For the electron pair experiment the detector was triggered by the deposition of more than 2 GeV of energy in each of the two lead-glass arrays. The energy in each array was further constrained by hardware to consist of at least 1.5 GeV in three adjacent columns and 1.5 GeV in three adjacent rows. Finally, the on-line software required that at least 1.5 GeV be recorded in a 3×3 block cluster. The cluster requirement was designed to reject events in which the energy in an array was due to several particles. The trigger did not include a charged particle requirement and was therefore sensitive to $\pi^0\pi^0$ pairs, which constitute the vast majority of the recorded events.

A trigger rate of 2-3/sec was the maximum consistent with off-line computer time availability. At the average luminosity of $\sim 3 \times 10^{31} \text{ cm}^{-2} \text{ sec}^{-1}$ at which these data were collected, this constraint dictated the level of the thresholds described above.

4. ANALYSIS AND CUTS

As explained in the previous section, the majority of the triggers consisted of $\pi^0\pi^0$ pairs. The first step in the data reduction was therefore to require a track coming from the intersection region to point within 12 cm of the centre of gravity of a 3×3 block energy-cluster in the lead glass. One such electron candidate was required in each array. The remaining events included electron pairs plus a background arising from

- i) charged hadrons depositing most of their energy in the lead glass by interacting in the coil or in the glass itself;
- ii) Dalitz decays and γ -ray conversions in the vacuum pipe and part of DCMI;
- iii) spatial overlaps of a π^0 providing the energy deposition in the lead glass, with a charged hadron providing the track.

Energy deposition from all these sources of background tends to be more spread out in space than that from an electron. To make use of this fact, the energy of the cluster was estimated in two ways. A measure of the energy E_9 was obtained by summing the nine blocks in the 3×3 block cluster. A second measure E_c was obtained by summing only those blocks intersected by a truncated cone with the track as its axis and with radii of 3 cm at the front face of the glass and 7.5 cm at a distance of 40 cm into the glass, as measured along the track. The ratio $RC = E_c/E_9$ is plotted in Fig. 2 for events where the two candidate tracks have opposite charge and for events where they have the same charge. This ratio was required to be greater than 0.98.

The majority of hadrons traverse the coil without interacting and give a pulse height in the B counter equivalent to single ionization (s.i.). Electrons, on the other hand, shower in the coil and give large pulse heights. One or the other of the two candidate electrons of a pair was required to have a pulse height in the B counter greater than 1.5 s.i. A charged hadron has a 35% probability of having a pulse height greater than 1.5 s.i., whereas an electron has a 78% probability.

In order to reject conversions in the A counters and the second half of DCML (0.025 radiation lengths in total), the candidate track was required to have at least one hit in DCML.

In some cases both members of a conversion pair (internal or external) were seen in the drift chambers. To reject these events, the effective mass of the candidate track with each of the other tracks in the event was formed in turn, assuming both particles were electrons. The distribution of these masses is shown in Fig. 3 for combinations where the second track has the opposite and the same charge as the candidate track. The plots have the same shape down to $150 \text{ MeV}/c^2$ in mass. Below this mass the events are predominantly of opposite charge. This difference is attributed to Dalitz decays and conversions. Candidate electrons were therefore rejected if they formed a mass of less than $150 \text{ MeV}/c^2$ with an associated track of opposite charge.

A characteristic of an electron is that its momentum p , as measured by the drift chambers, must equal the energy E , as measured by the lead glass within the accuracy of the two measurements. The energy as measured in the lead glass E_{obs} was corrected for energy loss in the coil and iron plate, assuming the observed particle was an electron. The following algorithm, developed during a study of the coil-B counter-glass response in a PS test beam, was used. The average correction applied was 0.28 GeV:

$$E = E_{\text{obs}} + 0.080 + 0.015 E_{\text{obs}} + 0.024(\text{PHB} - 2.5)$$

where E_{obs} is in GeV, and PHB is the pulse height in the B counter in units of s.i. The r.m.s. energy resolution of the lead glass is given by $\Delta E/E = 0.05 + 0.07/\sqrt{E}$, whereas the r.m.s. momentum resolution of the drift chamber/solenoid system is $\Delta p/p \sim 0.07 p$. The quantity E/p was computed for each candidate track. Electrons arising from conversion have $E/p > 1.0$ since the electron carries only a fraction of the π^0 energy and one electron is measured by the chambers to give p . On the other hand, the two gamma rays from a background π^0 merge in our apparatus into a single cluster. The energy measured by the lead glass is therefore that of the whole π^0 . The majority of overlaps also have $E/p > 1.0$ since in general the overlapping track is of low momentum. On the other hand, charged hadrons satisfying the trigger requirements tend to have E/p equal to or slightly smaller than 1.0. The higher the momentum of the hadron the larger is the probability of depositing a given amount of energy in the lead glass. However, this is outweighed by the fact that the p_T spectrum of hadrons is falling steeply. It is therefore those hadrons depositing most of their energy in the lead glass that are the main source of background. A plot of E/p for opposite charge and same charge events is shown in Fig. 4. For each candidate electron the uncertainty $\sigma_{E/p}$ on E/p arising from the measurement on E and p was computed, and the candidate particle was retained if the measured E/p was in the range

$$0 < E/p < 1 + 2 \sigma_{E/p} .$$

5. RESULTS

Data corresponding to an integrated luminosity = $3.5 \times 10^{37} \text{ cm}^{-2} \text{ sec}^{-1}$ have been analysed to date. Application of the above cuts resulted in 81 candidate pairs of opposite charge and 24 of same charge. The mass was calculated using the lead-glass energy. The resulting distributions are shown in Fig. 5. The drop below $6 \text{ GeV}/c^2$ is because of trigger thresholds. The background in the opposite sign pairs was assumed to be equal to the same charge pairs. A bin-by-bin subtraction can then be performed, and the cross-section was computed using

ρ = geometrical acceptance derived from Monte Carlo calculation assuming the production is flat in rapidity over the apparatus ($|y| < 0.7$),

= 0.10;

ϵ_{CH} = track reconstruction efficiency = 0.90 per track;

ϵ_{B} = efficiency of B counter cut = 0.95 per pair;

ϵ_{Ep} = efficiency of E/p cut = 0.98 per track;

ϵ_{RC} = efficiency of RC cut = 0.90 per track;

ϵ_{D} = efficiency of Dalitz and conversion cut. The only inefficiency would arise from the accidental vetoing of a genuine electron by an associated track. Only 10% of the events were removed by this cut, and it lost the same number of same and opposite charge pairs; ϵ_{D} was therefore taken to be 1.0.

The cross-sections $(d^2\sigma/dm dy)_{y=0}$ are tabulated in Table 1 together with the number of events and background events. The cross-sections are shown in Fig. 6 together with the data obtained at $\sqrt{s} = 62.4 \text{ GeV}$ by another ISR experiment⁴⁾. A fit derived from Fermilab data¹⁾ and scaled to $\sqrt{s} = 62.4 \text{ GeV}$ according to the scaling law $d\sigma/dm = (1/m^3)f(m/\sqrt{s})$ is also shown in Fig. 6 and is in very good agreement with the data.

Given the reported masses of the three Υ peaks⁵⁾ and the energy resolution of this experiment [$\Delta m (\text{FWHM}) = 1.25 \text{ GeV}/c^2$], the Υ region is defined as $8.75 \text{ GeV}/c^2$ to $11.0 \text{ GeV}/c^2$. Assuming all 15 events in this mass interval to be due to the Υ ,

$$B \left. \frac{d\sigma}{dy} \right|_{y=0} = (7.8 \pm 2.0) \times 10^{-36} \text{ cm}^2$$

or a factor of 30 ± 8 larger than the Fermilab result at $\sqrt{s} = 27.4$ GeV. Although the geometrical acceptance of the apparatus increases with mass and the experiment is sensitive to masses up to $60 \text{ GeV}/c^2$, no event was observed above $13 \text{ GeV}/c^2$.

The p_T distributions for the e^+e^- candidates and for the background are shown in Fig. 7 for two mass intervals:

- i) $6-8.75 \text{ GeV}/c^2$
- ii) $> 8.75 \text{ GeV}/c^2$.

After subtraction of the background, the mean p_T is found to be

$$1.67 \pm 0.21 \quad \text{and} \quad 1.65 \pm 0.20 \text{ GeV}/c$$

for the two mass intervals. These values are to be compared to a mean p_T of $1.2 \text{ GeV}/c$ obtained at Fermilab⁶⁾ for $6 < m < 8 \text{ GeV}/c^2$ at $\sqrt{s} = 27.4$ GeV. These values of the mean p_T can also be compared with the mean p_T of the $\pi^0\pi^0$ pairs in the same mass intervals, 2.1 ± 0.1 and $2.3 \pm 0.1 \text{ GeV}/c$, respectively.

Since the drift chamber system has a large acceptance ($\Delta\phi = 360^\circ$ and $\Delta\theta = 90^\circ \pm 45^\circ$) it was possible to measure the momentum spectrum and mean multiplicity of the tracks associated with the e^+e^- candidates. The transverse momentum spectra of positive and negative tracks are very similar and were therefore combined. This combined spectrum is shown in Fig. 8 for the two mass intervals described earlier. The transverse momentum spectra for tracks associated with $\pi^0\pi^0$ events with effective mass in the same two mass intervals are also shown. The three spectra are normalized in the bin $0.25-0.50 \text{ GeV}/c$. The spectra for the tracks associated with e^+e^- events appears to be steeper than the spectra for the tracks associated with $\pi^0\pi^0$ events.

The mean multiplicity of tracks associated with e^+e^- events is 6.1 ± 1.0 and 5.5 ± 1.0 for the two mass intervals, to be compared with 10.0 ± 0.2 and 9.5 ± 0.3 for $\pi^0\pi^0$ events.

REFERENCES

- 1) S.W. Herb et al., Phys. Rev. Letters 39 (1977) 252.
- 2) L. Camilleri et al., presented at the Wire Chamber Conference, Vienna, 1978, Proc. to be published in Nuclear Instrum. Methods.
- 3) J.S. Beale et al., Nuclear Instrum. Methods 117 (1974) 50.
- 4) J.H. Cobb et al., Phys. Letters 72 (1977) 273.
- 5) L.M. Lederman, Proc. Internat. Symposium on Lepton and Photon Interactions at High Energies, Hamburg, 1977 (DESY, Hamburg, 1977), p. 567.
- 6) D.M. Kaplan et al., Phys. Rev. Letters 40 (1978) 435.

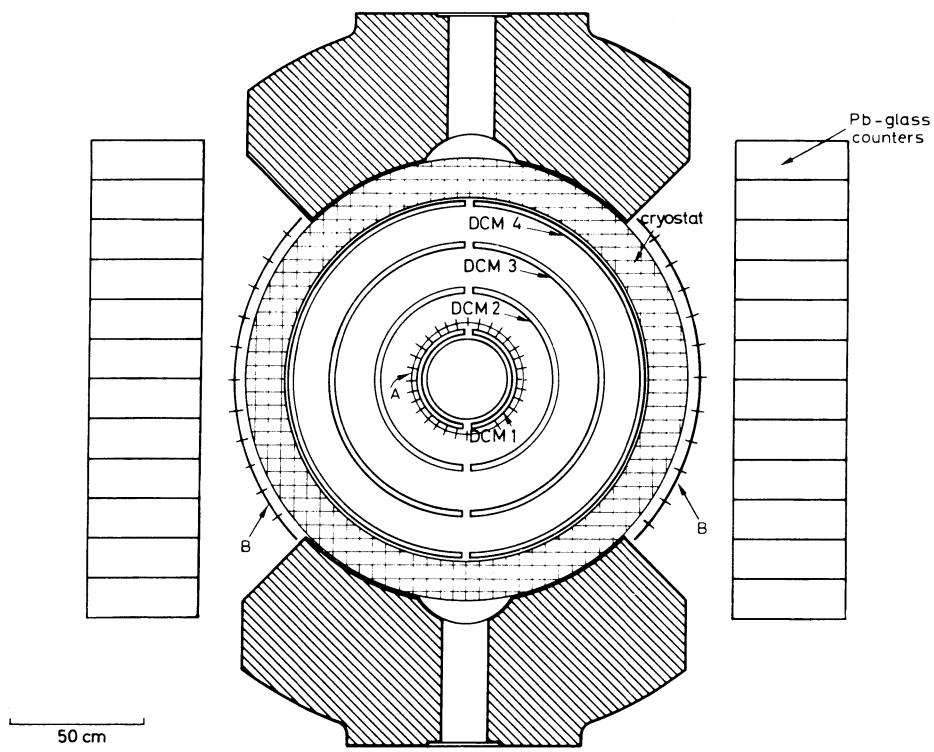
Table 1

Mass (GeV/c ²)	Number of events		Signal	τ (m/ \sqrt{s})	$(d^2\sigma/dm dy)_{y=0}$ (cm ² /GeV/c ²)
	Opposite sign	Same sign			
6.0-6.5	24	7	17 ± 5.6	0.100	(1.8 ± 0.6) × 10 ⁻³⁵
6.5-7.0	14	5	9 ± 4.3	0.108	(9.4 ± 4.5) × 10 ⁻³⁵
7.0-8.0	15	9	6 ± 5.0	0.120	(3.1 ± 2.5) × 10 ⁻³⁶
8.0-9.0	7	2	5 ± 3.0	0.136	(2.6 ± 1.6) × 10 ⁻³⁶
9.0-9.5	10	0	10 ± 3.2	0.148	(1.0 ± 0.33) × 10 ⁻³⁵
9.5-10.0	3	0	3 ± 1.7	0.156	(3.1 ± 1.8) × 10 ⁻³⁶
10.0-11.0	1	0	1 ± 1	0.168	(2.0 ± 2.0) × 10 ⁻³⁶
11.0-12.0	1	0	1 ± 1	0.184	(2.0 ± 2.0) × 10 ⁻³⁶

Figure captions

- Fig. 1 : a) The apparatus as viewed along the solenoid axis.
b) Top view of the apparatus.
- Fig. 2 : The ratio RC, as defined in the text, plotted for opposite charge and same charge electron pair candidates.
- Fig. 3 : Effective mass of candidate electrons with each of the other particles in the event. The distribution for combinations in which the other particle is of opposite charge to that of the candidate is plotted separately from the distribution in which the other particle is of same charge.
- Fig. 4 : The quantity E/p, defined in the text, plotted for opposite charge and same charge electron pair candidates.
- Fig. 5 : Mass distribution of opposite charge and same charge electron pair candidates.
- Fig. 6 : Differential cross-sections at $y = 0$, for e^+e^- production at $\sqrt{s} = 62.4$ GeV. The background has been subtracted.
- Fig. 7 : Distribution of the p_T of the e^+e^- candidates. The distributions are shown for candidates of opposite and same charge and for two mass intervals
- i) $6 < m_{ee} < 8.75$ GeV/c²
 - ii) $m_{ee} < 8.75$ GeV/c².
- Fig. 8 : The transverse momentum spectrum of particles associated with
- a) e^+e^- pairs
 - b) $\pi^0\pi^0$ pairs.

a)



b)

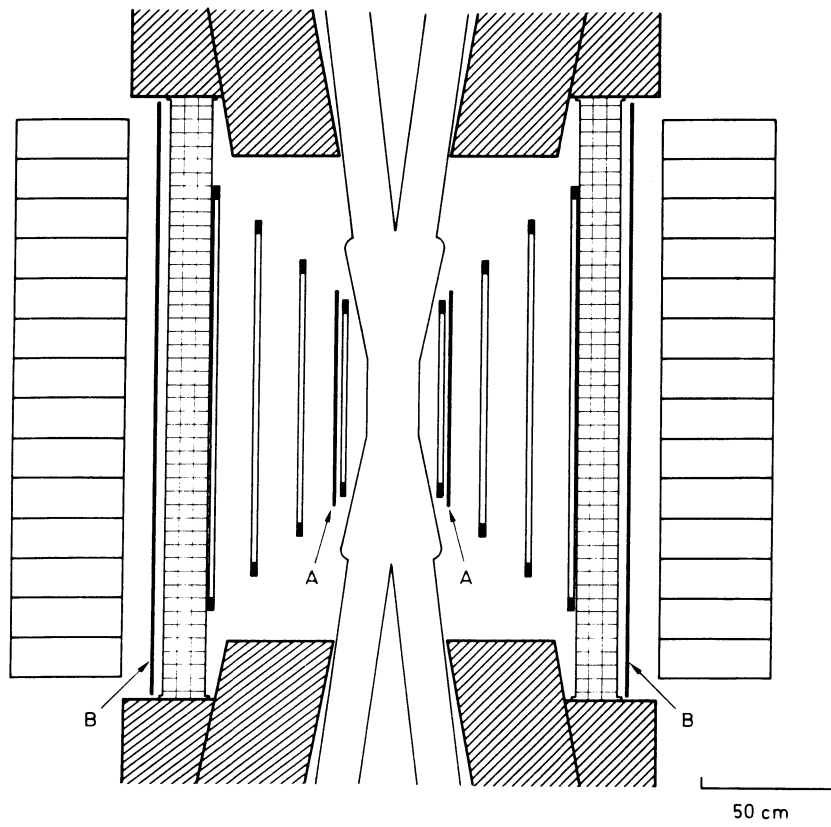
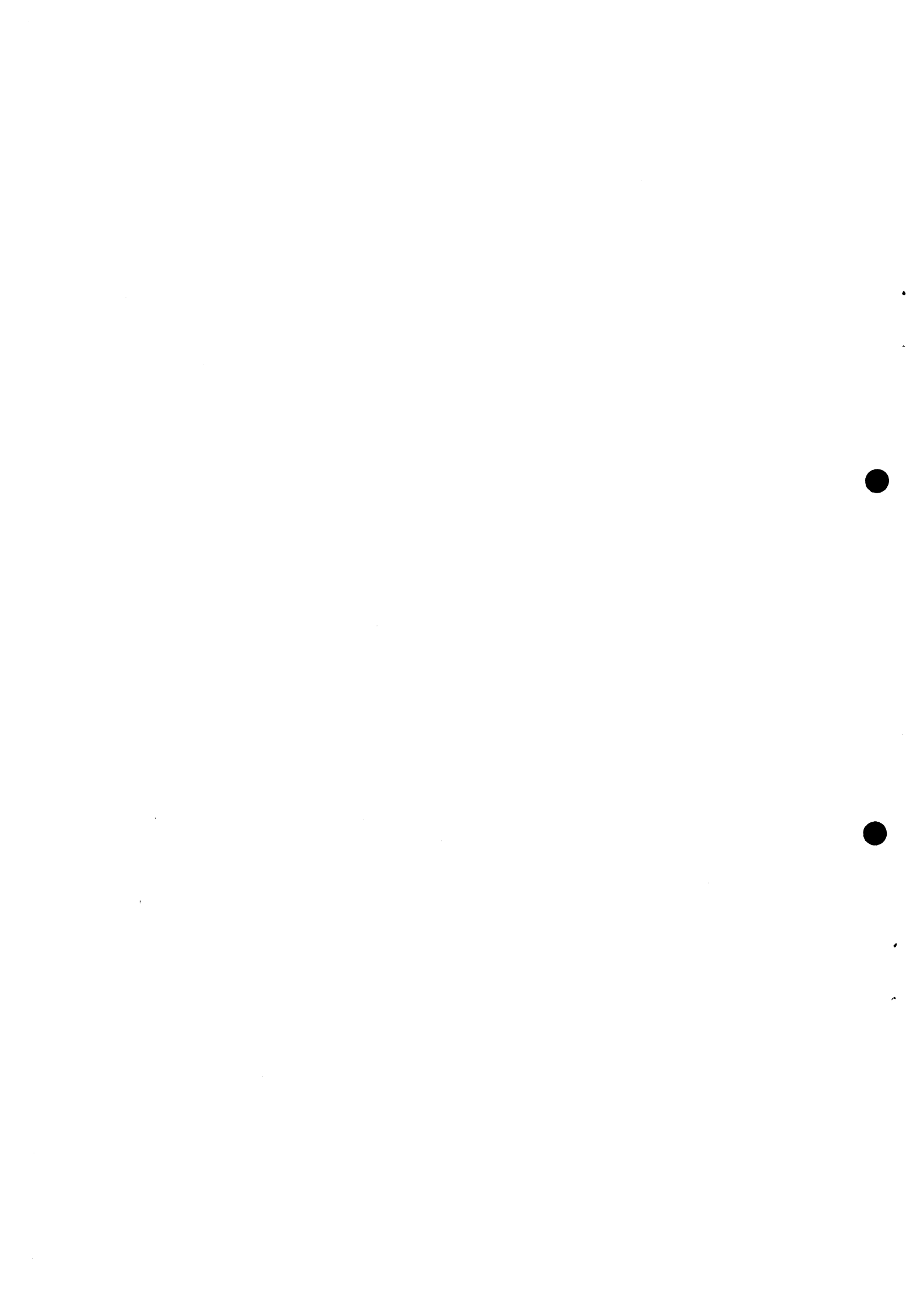


Fig. 1



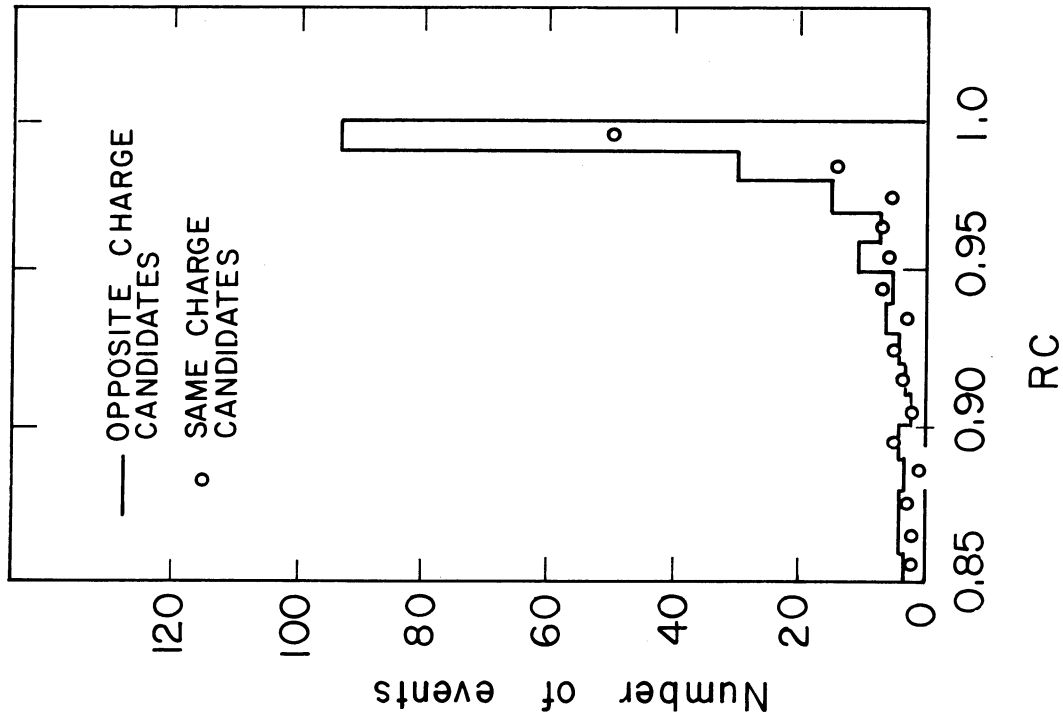


Fig. 2

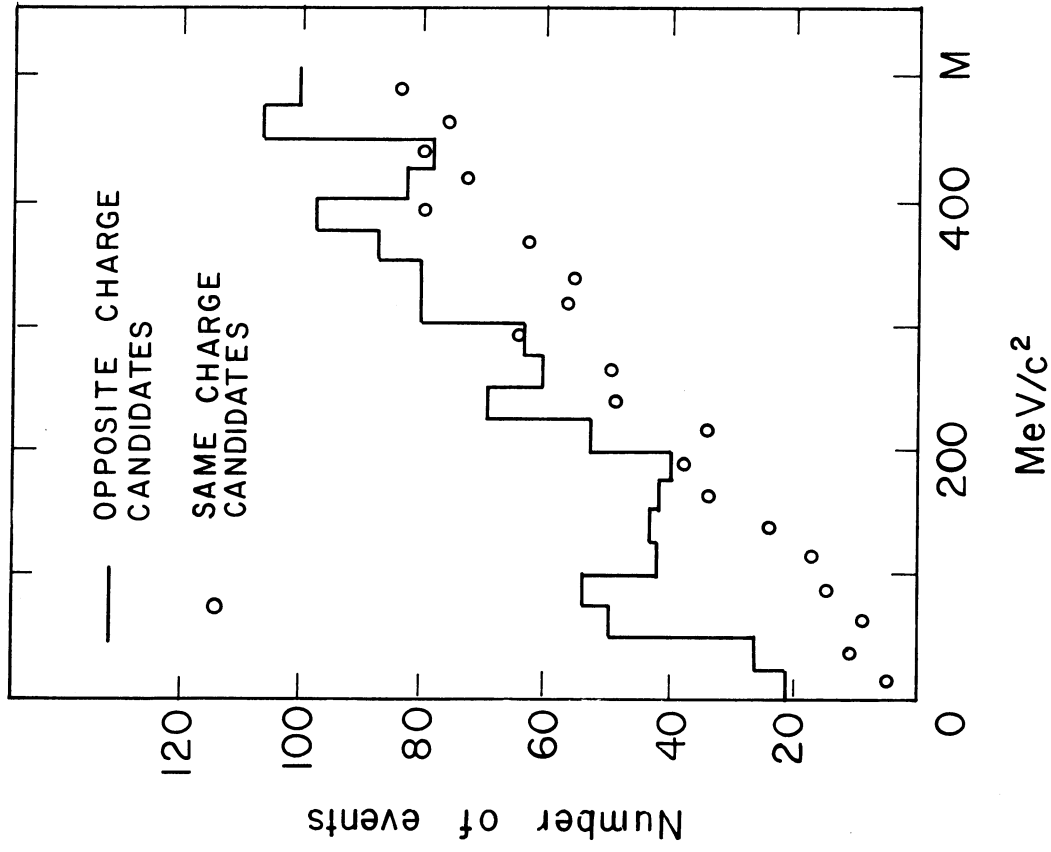


Fig. 3

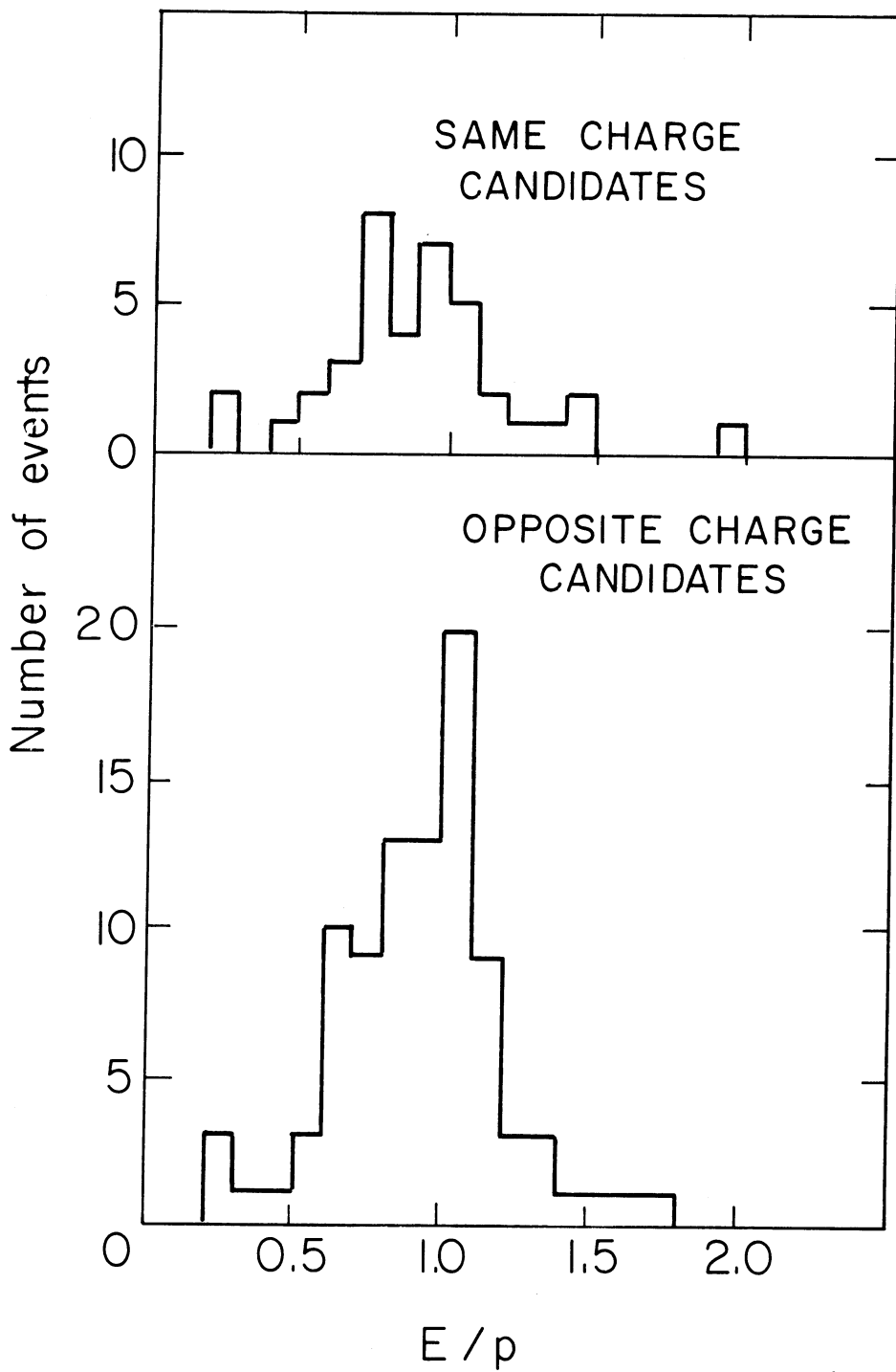


Fig. 4

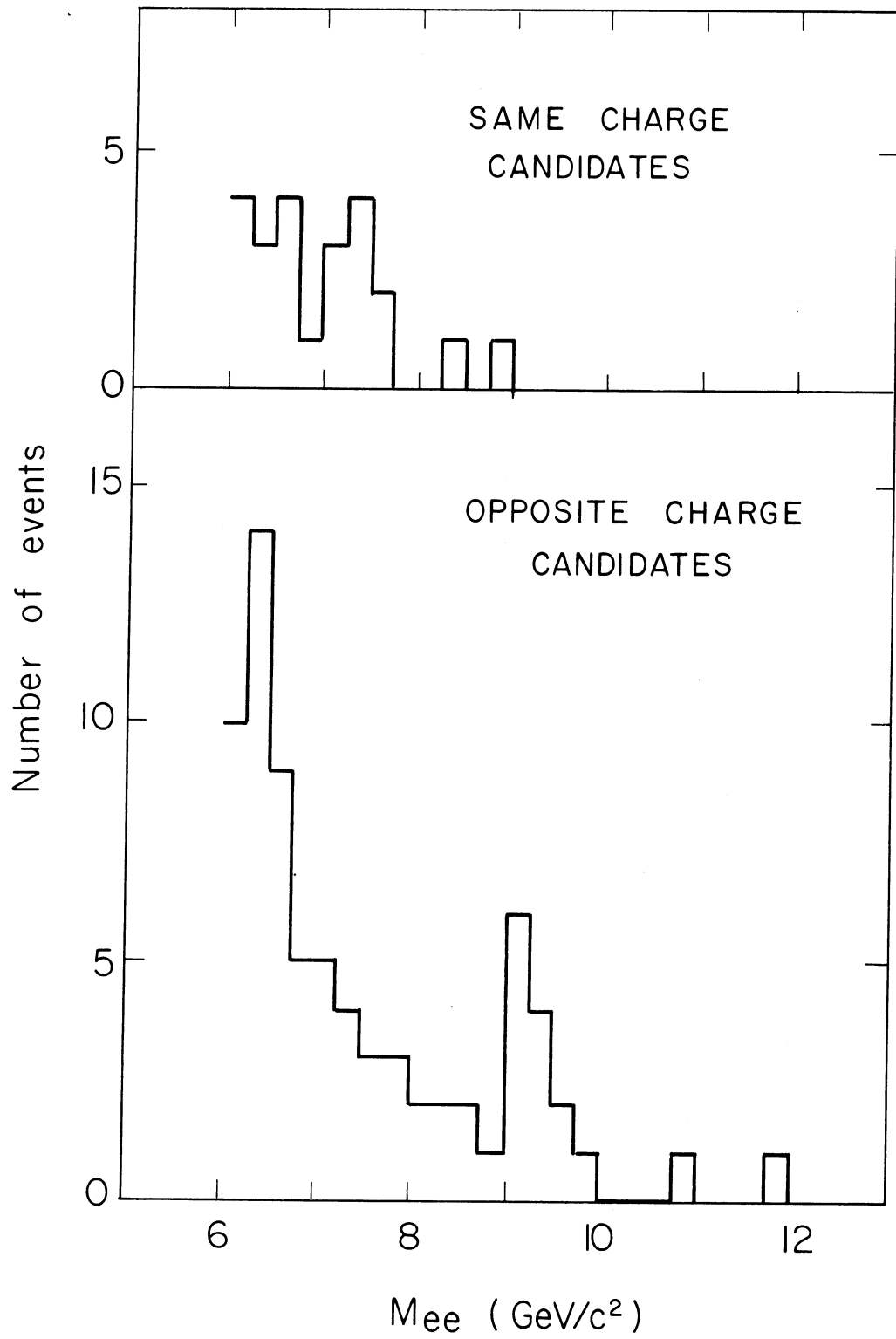


Fig. 5

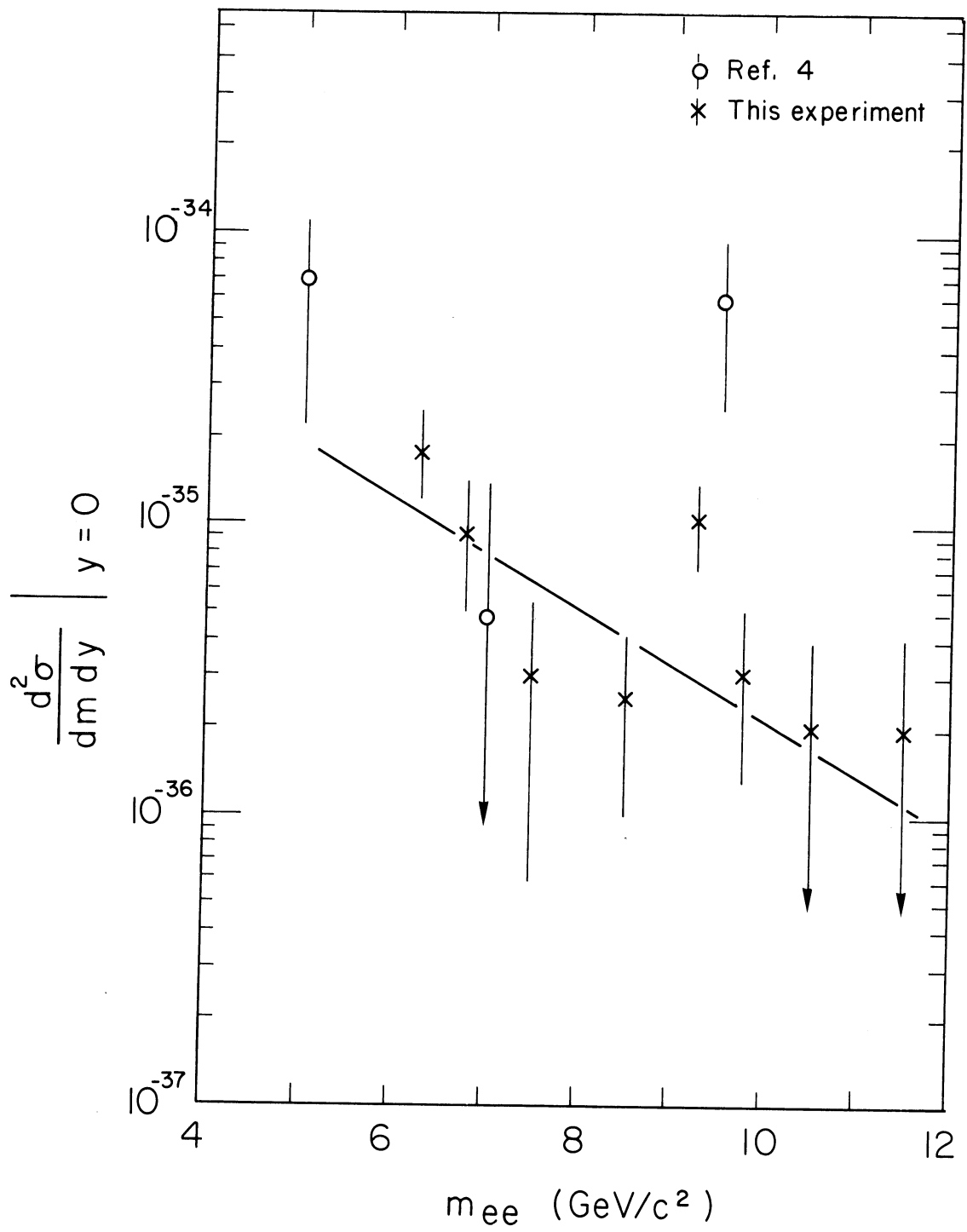


Fig. 6

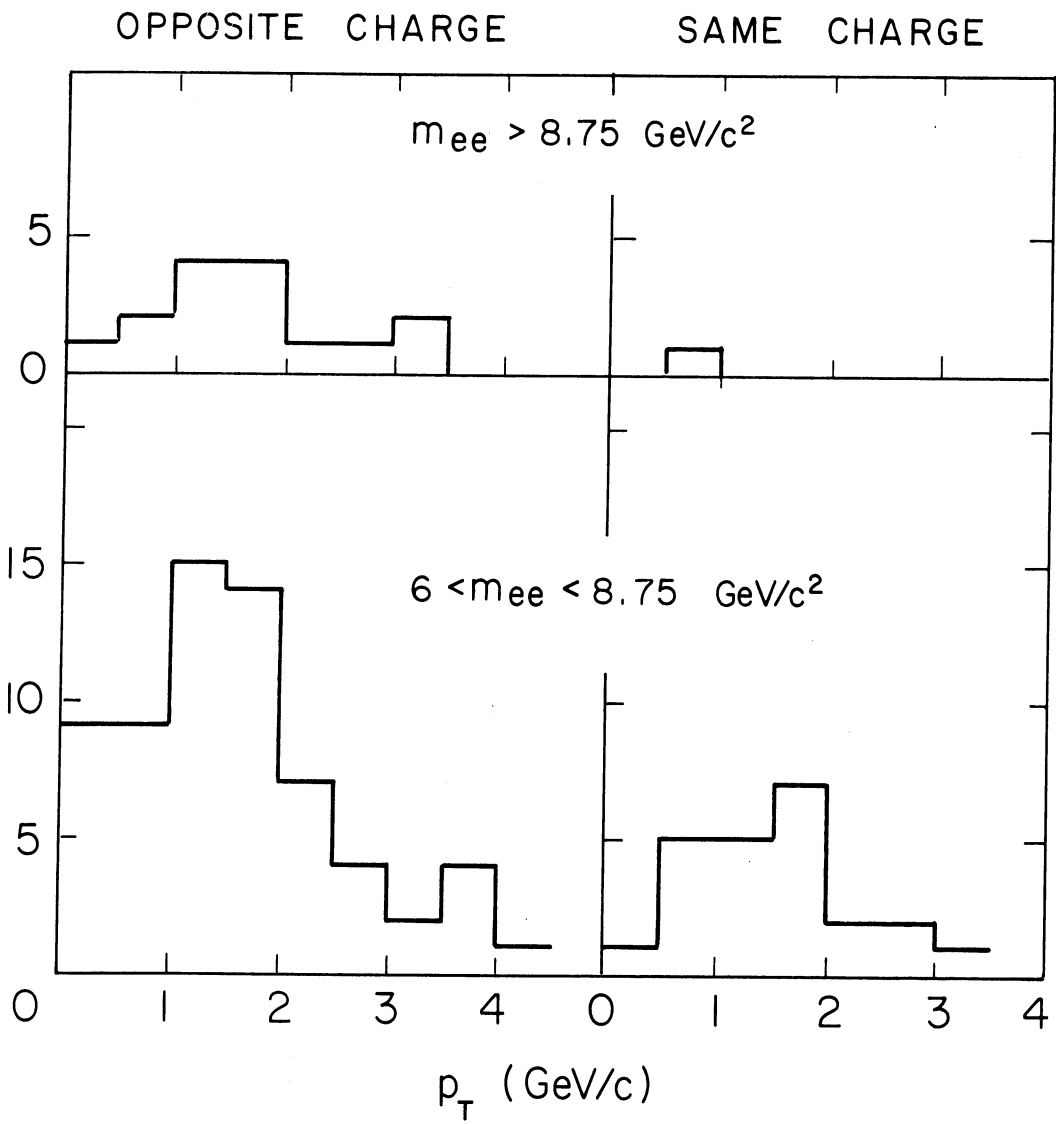


Fig. 7

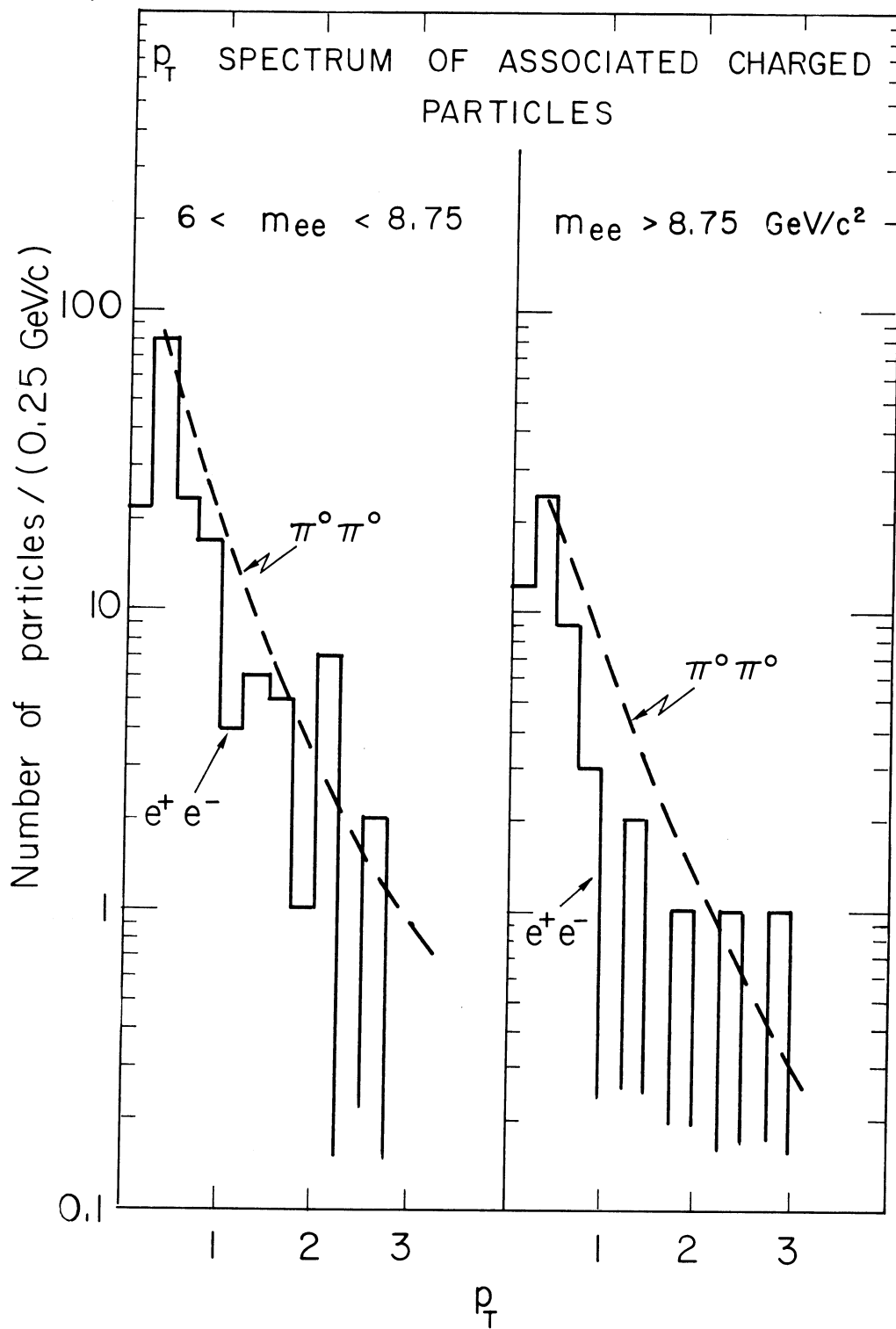


Fig. 8